RSC Advances

ROYAL SOCIETY OF CHEMISTRY

www.rsc.org/advances

Cadmium Selenide Quantum Dots Solar Cells Featuring Nickel Sulfide/Polyaniline as Efficient Counter Electrode Provide 4.15% Efficiency

Gentian Yue [a†,*], Furui Tan [a†], Jihuai Wu [b], Fumin Li [a], Jianming Lin[b], Miaoliang Huang[b], Weifeng Zhang[a]

[a] *Key Laboratory of Photovoltaic Materials of Henan and School of Physics & Electronics, Henan University, Kaifeng 475004, China*;

[b] *Institute of Material Physical Chemistry, Huaqiao University, Quanzhou 362021, China*

Keywords: Counter electrodes; cadmium selenide; quantum dots solar cells; photovoltaic performance

Abstract: Nickel sulfide decorated polyaniline (NiS/PANI) co-deposition onto fluorine-doped tin oxide (FTO) substrate by using an in situ electropolymerization route, and served as counter electrode (CE) for polysulfide electrolyte in cadmium selenide (CdSe) quantum dots sensitized solar cells (QDSSCs). The NiS/PANI CE provided great electrocatalytic activity and lower charge-transfer resistance compared to the platinum (Pt), NiS and PANI CEs under the same preparation condition prepared by using cyclic voltammetry (CV), electrochemical impedance spectroscopy (EIS), and Tafel polarization plots characterized. It was because the photoanode was modified with TiO_2 dense layer and thioglycolic acid that the QDSSC exhibited an improved fill factor and short-circuit current density. Under the optimum condition, the QDSSC featuring a NiS/PANI counter electrode provided an enhanced power conversion efficiency of 4.15% under illumination of 100 $mW \cdot cm^{-2}$.

† These authors contributed equally to this work and should be considered co-first authors.

∗ Corresponding author. +86 371 23881602, E-mail address: yuegentian@henu.edu.cn (G. Yue).

1. Introduction

Quantum dots sensitized solar cells (QDSSCs) have attracted increasing interest for the quantum dots have presented the possibility of band gap tunability, high extinction coefficient, large intrinsic dipole moments, and potential processes of multiple exciton generation. [1-4] Generally, QDs that absorb light in the visible region, such as cadmium sulfide (CdS), cadmium selenide (CdSe), lead selenide (PbSe), lead sulfide (PbS) QDs and so on, have been served as sensitizer in solar cells. [5-8] The advantages of the QDs compared to conventional dyes are their quantum-confinement effect, Auger recombination, and the miniband effect. [9-12] However, the reported conversion efficiency of QDSSCs is still far below their theoretical value (44%) and that of the DSSCs. [13-15] One major challenge in this field is how to assemble QDs into the mesoporous TiO_2 matrix to obtain a well-covered monolayer and the energy losses that occur at the interface of the counter electrode and electrolyte, which results in low short-circuit current and open-circuit photovoltage. [16,17] To

further increase the photovoltaic efficiency of QDSSCs, it appears that it will be necessary to develop new types of efficient counter electrode (CE) matched well with the QDs and electrolyte, which would resolve the severe problem of inner energy loss in QDSSCs and improve the fill factor.

In general, platinum (Pt) and gold (Au) CEs are not ideal catalytic materials in polysulfide electrolyte, mainly because their surface activity and conductivity are suppressed as a result of adsorption of the sulfur atoms. [18,19] Therefore, metal sulfides such as cobalt sulfide (CoS), nickel sulfide (NiS), and copper sulfide (CuS) have become promising candidates as catalysts for polysulfide redox reactions in photoelectrochemical cells. Cu_2S [20] and carbon based nanomaterials [21] have been used as CEs in QDSSCs, the fill factors of the QDSSCs were nearly 50%. Yang and his co-workers fabricated CdS/CdSe QDSSCs featuring cobalt sulfide (CoS) CE obtained power conversion efficiency (*PECs*) as high as 3.4%. [22] Furthermore, the composite materials consisted of carbon materials, organic conducting polymers or transition metal compounds with great electrocatalytic ability in iodide/triiodide (I^-/I_3^-) electrolyte served as CEs in DSSCs and achieved an enhanced power conversion efficiency. [23-26] It can be inferred that the electrocatalytic property of the composite CEs made from organic conducting polymers and metal sulfides will be improved greatly thinking along this line.

Thus, a novel nickel sulfide decorated polyaniline (NiS/PANI) composite counter electrode was prepared onto fluorine-doped tin oxide (FTO) substrate by using an in situ electropolymerization route. The NiS/PANI CE showed excellent electrocatalytic activity and low charge transfer resistance relative to that of Pt CE in sulfide/polysulfide (S^{2-}/S_n^{2-}) electrolyte, which were demonstrated by the results of cyclic voltammetry (CV) and electrochemical impedance spectroscopy (EIS). TiO_2 anode surface was modified by immersing in 0.1 M thioglycolic acid (TGA) as the bridge TiO_2 surface and the QDs, and next CdSe QDs were spin-coated on modification of TiO_2 substrate. A new QDSSC assembled with the NiS/PANI CE and polysulfide electrolyte exhibited a considerably enhanced performance in power conversion efficiency of 4.15% under irradiation of 100 $mW \cdot cm^{-2}$ (AM 1.5).

2. Experimental

2.1 Preparation of the NiS/PANI CEs

The preparation of the NiS/PANI CE by using a two-step cyclic voltammetry approach outlined as following. Firstly, the electrodeposition of PANI onto FTO substrate was carried out with an electrochemical analyzer system. All experiments were implemented in a three-electrode cell at room temperature (about 25℃), including one Pt foil as counter electrode, one Ag/AgCl electrode as reference electrode and FTO substrate with an exposed area of 0.8×1 cm^2 as the working electrode. The base polymerization solution of PANI consisted of 0.5 M aniline and 1.0 M perchloric acid ($HClO_4$) solution. A constant potential of −1.2 V vs. Ag/AgCl was employed for the electrodeposition of PANI on FTO substrate. The obtained PANI CE was put into anhydrous ethanol for 0.5 h, then modified by 4-ATP/ethanol solution for 10 min and vacuum oven at 80□ for 12 h. Secondly, the obtained PANI CE as the working electrode soaked 0.05 M nickel (II) chloride hexahydrate ($NiCl_2 \cdot 6H_2O$, 98%) and 1.0 M thiourea (TU, ≥ 99.0%) solution to carry out the deposition procedure. The FTO coated with NiS/PANI film was put into anhydrous ethanol for 0.5 h and vacuum oven at 80□ for 12 h, respectively. Then, the NiS/PANI counter electrode was obtained. For comparison, the Pt, PANI and NiS electrodes were prepared by using a similar three-electrode system under the same parameter setting. The Pt electrode was obtained from the 0.01 M H_2PtCl_6 ethanol solution to carry out the electrodeposition procedure.

2.2 Synthesis of CdSe QDs

CdSe QDs were synthesized as follows. A cadmium (Cd) precursor solution (1 mmol of cadmium oxide dissolving in 3 ml of oleic acid together with 3g tri-n-octylphosphine oxide) was heated to 140□ for 1 h under nitrogen protection. In another flask, a selenium (Se) source solution was for med by dissolving 1.0 mmol of Se powder in 3 ml tri-noctylphosphine. The Cd stock solution was heated to 260℃, and then the Se solution was quickly injected. The reaction proceeded for 3~4 min at 260□ to produce CdSe QDs with diameter of 3~4 nm. The CdSe QDs were purified with chlorobenzene/ethanol solvent/antisolvent for at least last four times and finally dissolved in chlorobenzene.

2.3 Fabrication of QDSSC

A TiO_2 anode was prepared as our previous studies. [27,28] The obtained TiO_2 anode with dense layer was modified by TGA, which was commonly used as the bridge between TiO_2 anode surface and the QDs.[29] The

CdSe QDs was spin-coated on modification of TiO_2 substrate at 500 rpm for 10 s and at 1500 rpm for 30 s. Four spin-coating processes were carried out on the substrate. Thus the CdSe-sensitized TiO_2 anode with thickness of 2-3 μm was obtained. The QDSSC was fabricated by injecting the S^{2-}/S_n^{2-} electrolyte (methanol and distilled water solution (vol. ratio: 7/3) contained of 2 M S, 0.5 M Na_2S and 0.2 M KCl) in the aperture between the CdSe-sensitized TiO_2 electrode and the NiS/PANI CE. The two electrodes were clipped together and wrapped with thermoplastic hot-melt Surlyn.

2.4 Characterization

The surface morphology of the sample was observed by using JSM-7001F field emission scanning electron microscope (SEM). The morphology of CdSe nanoparticles was confirmed by transmission electron microscopy (TEM) on a Hitachi H-800 (Hitachi, Ltd., Tokyo, Japan) at an acceleration voltage of 80 kV. CV measurements of the samples were taken in a three-electrode one-compartment cell with the sample electrode as working electrode, a Pt foil as counter electrode and Pt wire as reference electrode dipped in the S^{2-}/S_n^{2-} electrolyte. CV and EIS were conducted by the use of a computer-controlled electrochemical analyzer (CHI 660E, Shanghai Chenhua Device Company, China) (scan conditions: 40-200 $mV \cdot s^{-1}$). The electrolyte used in the QDSSC test was also injected into the dummy cells for the EIS measurements. EIS was carried out under the simulating open-circuit conditions at ambient atmosphere, sealing with thermoplastic hot-melt Surlyn and leaving an exposed area of 0.64 cm^2. The frequency of applied sinusoidal AC voltage signal was varied from 0.1 Hz to 10^5 Hz and the corresponding amplitude was kept at 5 mV in all cases.

The photovoltaic test of QDSSC with an exposed area of 0.4×0.5 cm^2 was carried out by measuring photocurrent-photovoltage (*J-V*) character curve under white light irradiation of 100 $mW \cdot cm^{-2}$ (AM 1.5 G) from the solar simulator (XQ-500W, Shanghai Photoelectricity Device Company, China) in ambient atmosphere. The fill factor (*FF*) and the photo-electric conversion efficiency (*PCE*) of QDSSC were calculated according to the following equations:

$$PCE\ (\%) = \frac{V_{max} \times J_{max}}{P_{in}} \times 100\% = \frac{V_{oc} \times J_{sc} \times FF}{P_{in}} \times 100\% \qquad (1)$$

$$FF = \frac{V_{max} \times J_{max}}{V_{oc} \times J_{sc}} \quad (2)$$

where J_{sc} is the short-circuit current density (mA·cm^{-2}); V_{oc} is the open-circuit voltage (V); P_{in} is the incident light power (mW·cm^{-2}); J_{max} (mA·cm^{-2}) and V_{max} (V) are the current density and voltage at the point of maximum power output in the *J-V* curve, respectively.

3. Results and discussions

3.1 Surface morphology and composition of the samples

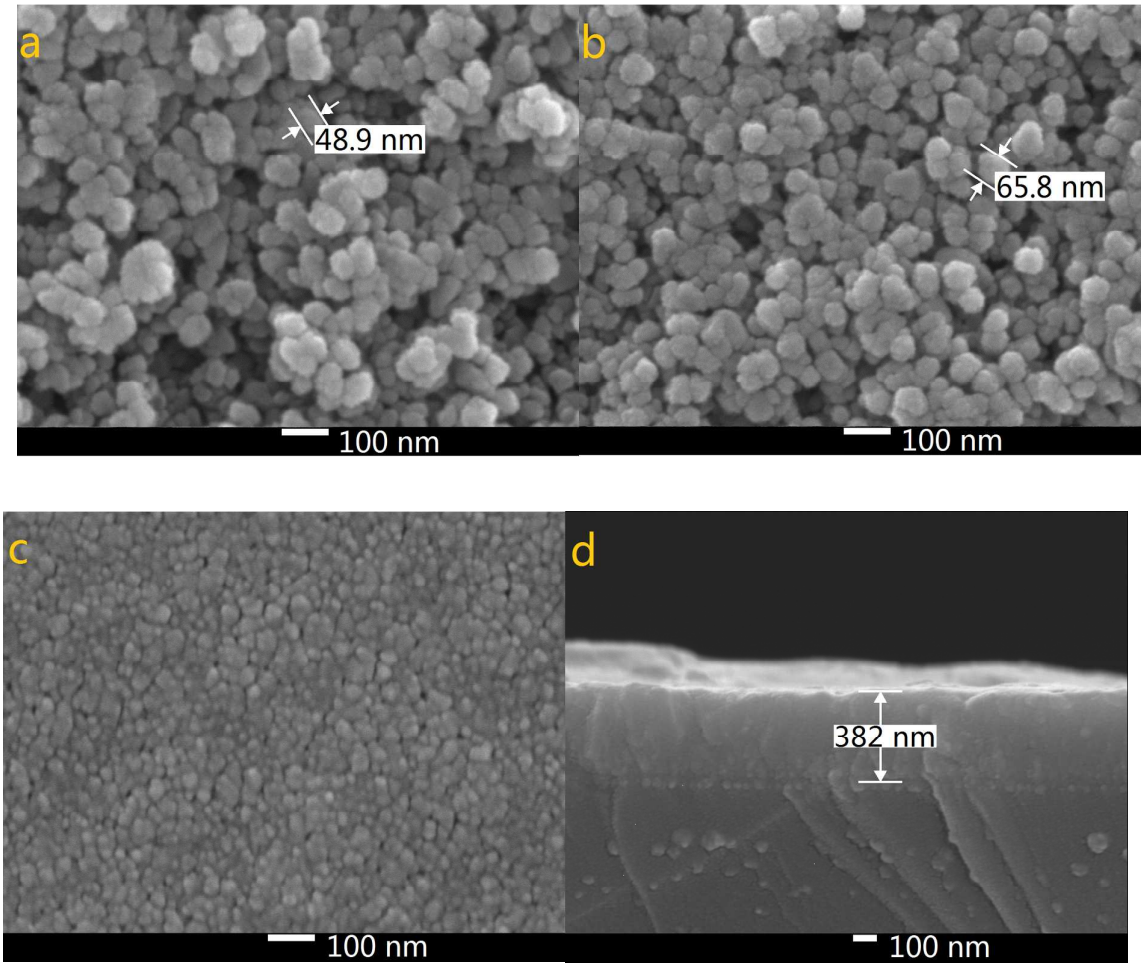

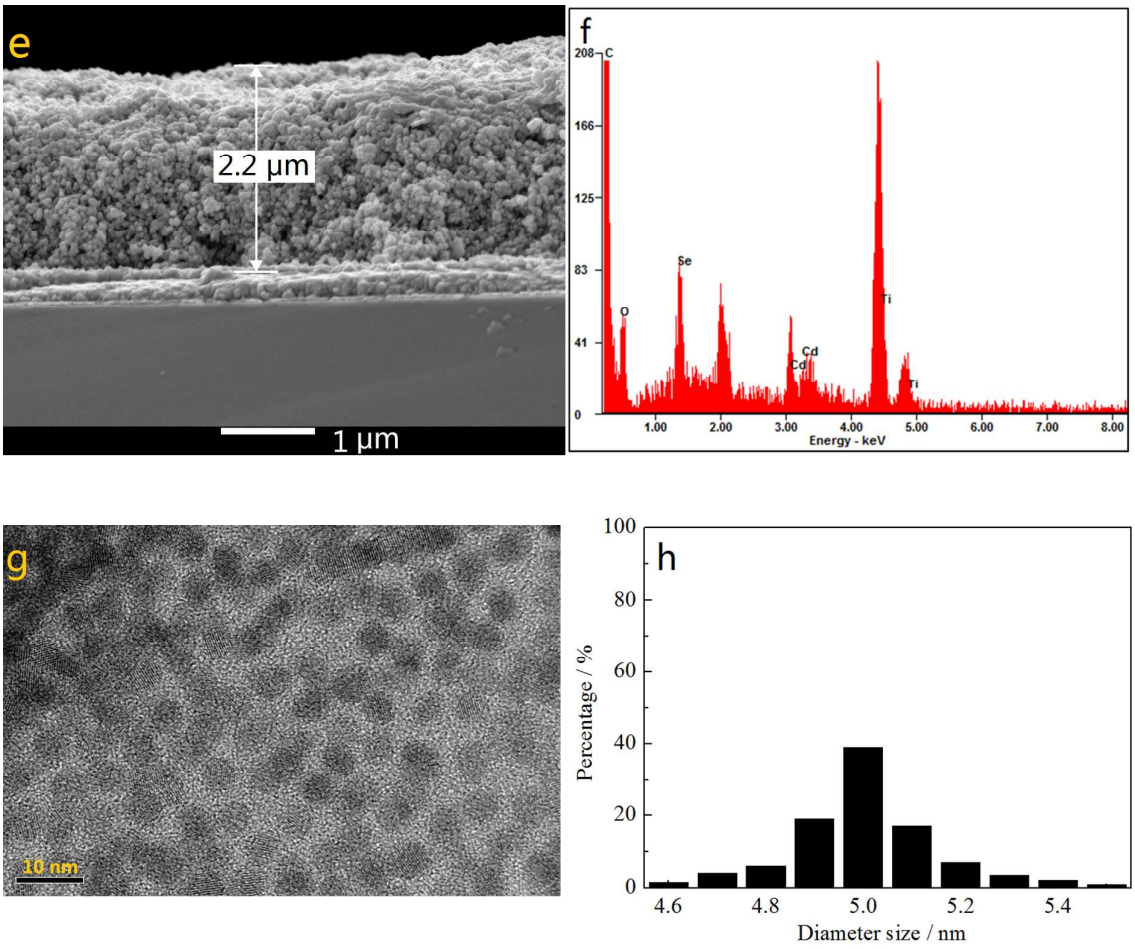

Fig. 1 The SEM images of pure TiO_2 (a), TGA decorated CdSe@TiO_2 (b); TiO_2 dense layer (c); the cross-sectional of TiO_2 dense layer (d) and pure TiO_2 (e); the EDS of the TGA decorated CdSe@TiO_2 (f); the TEM image of CdSe QDs (g) and the histogram analysis of particle size distribution (h).

Fig. 1a and b show the SEM images of TiO_2 films without and with modification of TGA and CdSe QDs. As the electron-extracting layer, the porous and loose nanostructure of pure TiO_2 film (particle size of ~49 nm in diameter as highlighted in Fig. 1a) with the thickness of about 2.2 μm (Fig. 1e) will allow a large number of S^{2-}/S_n^{2-} electrolyte to permeate into TiO_2 film and make a well contact with counter electrode. The TGA decorated CdSe@TiO_2 nanoparticles with the larger size (particle size of □65 nm in diameter as shown in Fig. 1b) than that of the pure TiO_2 nanoparticles, signaling to the word that TGA and CdSe QDs have successfully coated on the TiO_2 nanoparticles. The TiO_2 dense layer with thickness of about 382 nm and size of about 20 nm (Fig. 1c and d) was prepared by using a spin-coated method to reduce the charge recombination and improve the fill factor of the QDSSC. The EDS analysis for the CdSe@TiO_2 electrode

modification by TGA was carried out to identify the compositions of the samples. Fig. 1f indicates that the presence of C, O, Ti, Se, S and Cd elements in the CdSe@TiO_2 electrode. Among the elements, the large amount of Ti and O are responsible for the TiO_2, and C element comes from the carbon double sided tape; a little S comes from the TGA modification on the TiO_2 surface; Se and Cd elements are provided by the CdSe QDs. The results further demonstrate that the CdSe@TiO_2 electrode is successfully prepared by means of the facile route on FTO substrate. Furthermore, Fig. 1g and h display the TEM image of the CdSe Qds and the histogram analysis of particle size distribution. It can be seen that CdSe QDs with spherical structure have uniform shape and size, including predominantly them with diameter size of about 5.0 nm.

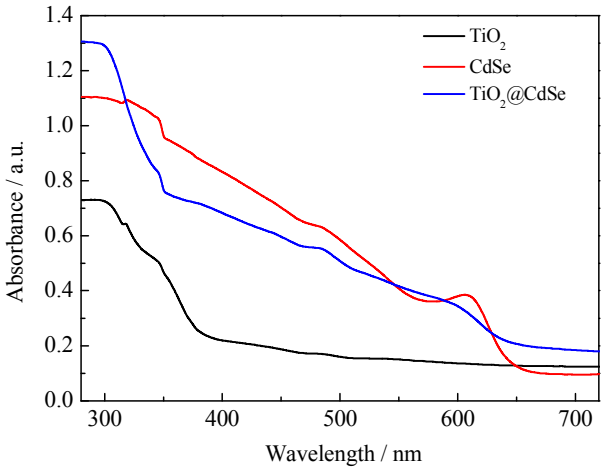

Fig. 2 The UV-vis absorption spectra of TiO_2, CdSe and CdSe@TiO_2 films.

The UV-vis absorption spectra of TiO_2, CdSe and CdSe@TiO_2 are displayed in Fig. 2. As expected, TiO_2 has no absorption band in visible range and shows the characteristic spectrum with its fundamental absorption of Ti–O bond in ultraviolet light range from 300 to 400 nm. CdSe QDs show their absorption range from 575-669 nm and distinct exciton absorption near 610 nm. Thus, the band gap calculated from the absorption edge is about 1.81 eV and the mean size of CdSe crystallites estimated from the excitonic peak is about 5.1 nm, which is well consistent with the histogram analysis of particle size distribution made from the TEM images. The CdSe@TiO_2 sample shows a phenomenon of light absorption superposition, in which the former band from 300 to 400 nm is assigned to the characteristic absorption of TiO_2, the latter band with an absorption peak of 609 nm is attributed to the electron transition from the valence bond (HOMO) to the conduction band (LUMO) of CdSe QDs. Consequently, the light response of CdSe QDs will help to increase

the concentration of photo-generated excitons so that larger photocurrent is expected after the excitons are split at the interface of hybrid bulk-heterojunction. [30-32]

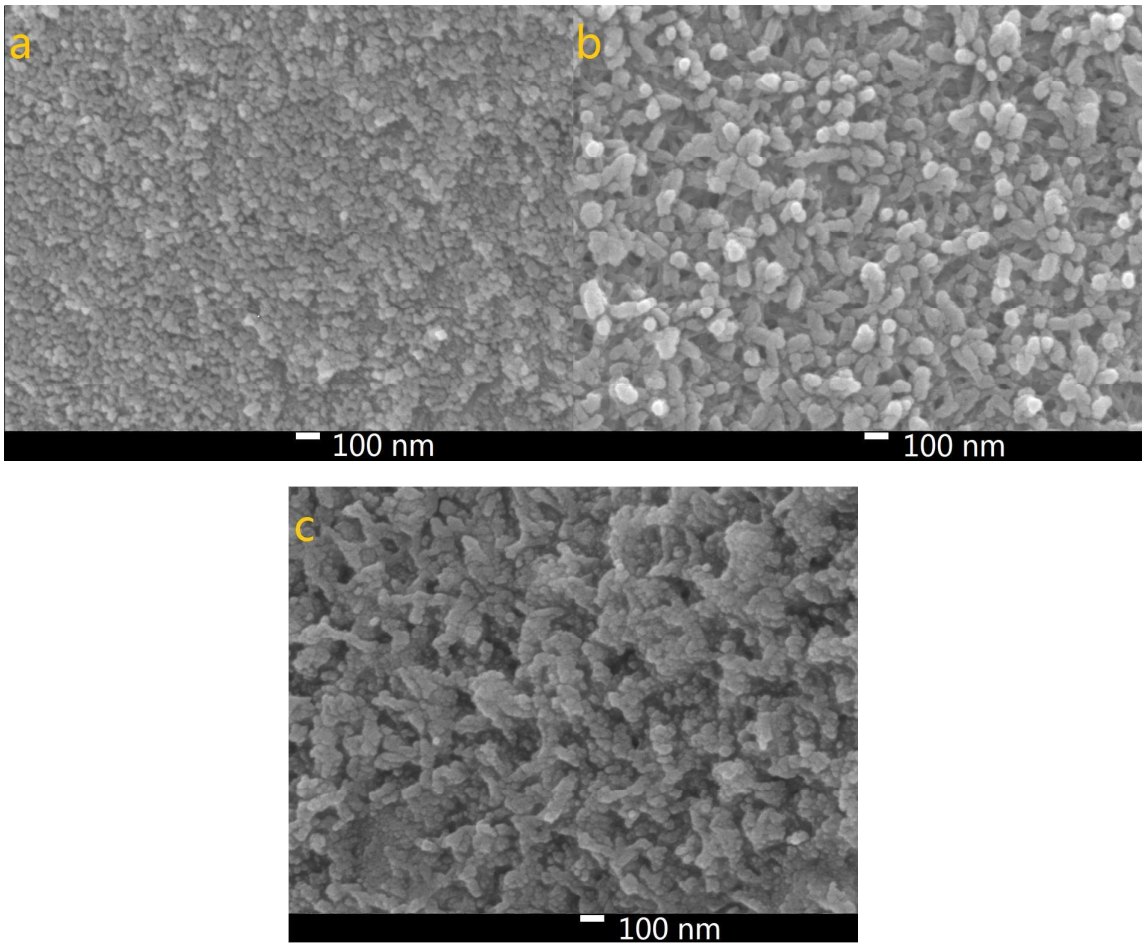

Fig. 3 The SEM images of NiS (a), PANI (b), and NiS/PANI (c).

Fig 3 shows the morphology of the NiS, PANI and NiS/PANI CEs. Fig 3a exhibits that NiS nanoparticles with the size of about 40 nm uniformly arranged on FTO substrate with perfect smooth surface. Fig 3b displays the PANI film composed of highly uniform and rough nanofibers with the diameter of 53.8 nm prepared by using the electrochemical deposition method. To effectively utilize the large active surface area of the PANI nanofibers and greatly improve the contact between the electrolyte and CE, the composite film consisted of PANI loading NiS is synthesized by using an electropolymerization approach. Notably, after loading NiS onto the PANI surface, the diameter of NiS/PANI increases to about 100 nm as shown as Fig 3c. The NiS/PANI CE with net-work structure provides highly effective contact between the CE and the S^{2-}/S_n^{2-} electrolyte, thus will possibly improving penetration of S^{2-}/S_n^{2-} electrolyte into the inside of the NiS/PANI

film and ultimately produces an enhancement performance for QDSSC.

3.2 Electrochemical properties

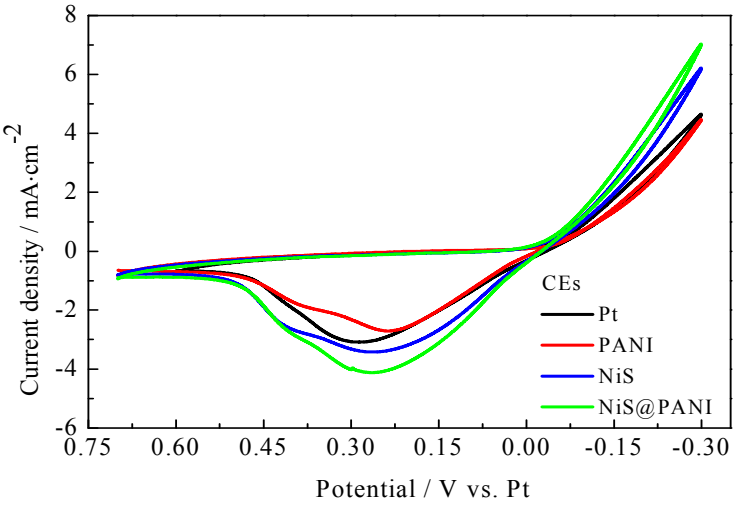

Fig. 4 Cyclic voltammograms for the various CEs with the scan rate of 50 $mV \cdot s^{-1}$.

Fig. 4 presents the CVs of the Pt, NiS, PANI and NiS/PANI CEs under S^{2-}/S_n^{2-} electrolyte system at scan rate of 50 $mV \cdot s^{-1}$. In the literature, although the exact chemical species and chemical mechanisms involved in a polysulfide electrolyte are very complicated and presently not well understood, it was reported that S^{2-} has an intimate relationship to the hole-recovery in a photoelectrochemical system. [33] The oxidized QDs is reduced back by S^{2-} ions in the electrolyte, the presence of sulfur simultaneously reacts with S^{2-} leading to the formation of polysulfide (S_n^{2-}, n=2-5), and the produced S_n^{2-} ions are then reduced at the CE; the S_n^{2-} plays as an electron acceptor to receive electron from counter electrode. Thus, redox reactions both at the photoanode and at the CE can be represented and through the following reaction: [34,35]

$$S_n + 2e^- \rightarrow S_n^{2-} \quad (3)$$

$$S_n^{2-} + 2e^- \rightarrow S_{n-1}^{2-} + S^{2-} \quad (4)$$

Consequently, the peaks in the CV curves quantitatively explain the catalytic reaction at the interface of the CE/electrolyte as follows. To our knowledge, in CV curves, the cathodic peak current density (I_{pc}) and the cathodic peak potentials (V_{pc}) are vital for the performance of CE and QDSSC, in which the I_{pc} is positive correlated with the reaction rate of the catalyst; and V_{pc} is inversely correlated with the electrocatalytic

activity of the CEs. The high I_{pc} indicates good electrocatalytic ability for CE in S^{2-}/S_n^{2-} electrolyte. It noticed that the NiS/PANI electrode shows the highest I_{pc} than that of the Pt, NiS and PANI electrodes in Fig.4, indicating the NiS/PANI electrode effectively acted as a catalyst in the reaction of the S^{2-}/S_n^{2-} redox couples. Also, the I_{pc} of the Pt electrode is lower than that of the NiS electrode. This indicates that the NiS CE has a better electrocatalytic ability than that of the Pt electrode because of the adsorb preferably and strongly of sulfur compounds on the Pt CE surface. The NiS and NiS/PANI CEs have a similar V_{pc} but smaller than that of the Pt electrode, meaning the excellent electrocatalytic ability for the NiS and NiS/PANI CEs in S^{2-}/S_n^{2-} electrolyte. Although smallest V_{pc} of PANI has proved compared to the above mentioned CEs (shown in Table 1), the catalytic activity of PANI still is worst for its low I_{pc}. Other possible reason of the enhanced catalytic activity for NiS/PANI CE includes the nanostructure has large surface area and could increase the catalytic activity of the CEs for polysulfide reduction. The high catalytic activity caused by the conversion rate of S^{2-} ions is more from oxidized S_n^{2-} ions and tends to result in high current density. [22]

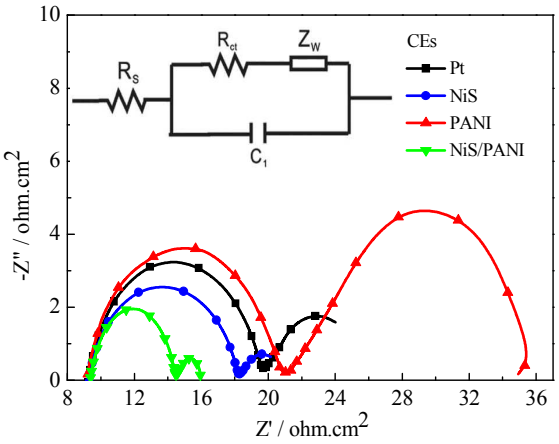

Fig. 5 Nyquist plots of the symmetrical CEs for S^{2-}/S_n^{2-} electrolyte and the relevant equivalent circuit model.

The typical Nyquist plots of the symmetrical Pt, NiS, PANI and NiS/PANI CEs in S^{2-}/S_n^{2-} electrolyte and the equivalent circuit are presented in Fig. 5, in which the series resistance (R_s) indicates by the high frequency nonzero intercept of the real axis; the first semicircle at high frequency refers to the charge-transfer resistance (R_{ct}) at the CE|electrolyte interface, and the second semicircle at low frequency represents the Nernst diffusion impedance (Z_w) corresponding to the diffusion resistance of the redox couple in electrolyte, respectively. [35,36] The R_s values of the Pt, NiS and PANI CEs are 9.25±0.01, 9.31±0.01 and

9.22±0.01 Ω·cm^2, respectively, which are similar to the R_s value of the NiS/PANI electrode (9.38±0.01 Ω·cm^2). These reflect a good bonding strength between Pt, NiS, PANI, NiS/PANI films and FTO substrates, which will effectively conduct electrons from counter electrode to electrolyte. The R_{ct} values of Pt, NiS, PANI and NiS/PANI CEs are found to be 10.47±0.01, 8.97±0.01, 11.86±0.01, and 5.13±0.01 Ω·cm^2, respectively. The lower value of R_{ct} usually corresponds to an improvement in the electrocatalytic activity of CE, resulting in acceleration of the higher electron transfer process at the electrolyte/CE interface. [37] The Z_w values of the Pt, NiS, PANI and NiS/PANI CEs are obtained to be 6.12±0.01, 2.72±0.01, 14.27±0.01, and 1.44±0.01 Ω·cm^2, respectively. The lower Z_w value of the CE indicates higher electrolyte diffusion, fast mass transfer of the electrons, and improved performance of the QDSSC. In a word, these data shows that the NiS/PANI CE is a good choice for use with the polysulfide electrolyte in QDSSC, and it offers the smallest charge-transfer resistance compared to Pt, NiS, and PANI CEs, along with superior solar cell functionality.

Table 1 The electrochemical performance parameters obtained from EIS and CV based on the various counter electrodes.

CEs	R_s (Ω·cm^2)	R_{ct} (Ω·cm^2)	Z_w (Ω·cm^2)	I_{pc} (mA·cm^{-2})	V_{pc} (V)
Pt	9.25±0.01	10.47±0.01	6.12±0.01	-3.016±0.001	0.25±0.01
NiS	9.31±0.01	8.97±0.01	2.72±0.01	-3.409±0.001	0.26±0.01
PANI	9.22±0.01	11.86±0.01	14.27±0.01	-2.721±0.001	0.27±0.01
NiS/PANI	9.38±0.01	5.13±0.01	1.44±0.01	-4.144±0.001	0.23±0.01

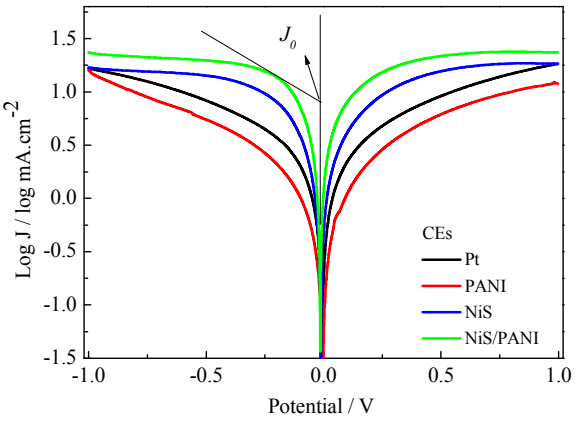

Fig. 6 Tafel curves of the various counter electrodes.

Fig. 6 exhibits the Tafel curves of Pt, NiS, PANI and NiS/PANI CEs. The curves at low potential (|U|< 0.120 V) correspond to the polarization zone and present the logarithmic current density as a function of the

potential. [38] The exchange current density (J_0) is obtained as the intercept of the extrapolated linear region of the curve when the over-potential is zero, which is inversely related to R_{ct} as illustrated in Eqn. (5), [39] and is therefore considered as a quantitative factor for evaluating the electrocatalytic activity of a CE.

$$J_0 = \frac{RT}{nFR_{ct}} \quad (5)$$

where R is the gas constant; n is the number of electrons involved in the reduction of S_n^{2-} at the electrode; T is the temperature; F is Faraday's constant; R_{ct} is the charge transfer resistance; C is the S_n^{2-} concentration.

Thus, according to the slopes for the anodic or cathodic branches of Fig. 6, the J_0 follows the order of NiS/PANI > NiS > Pt > PANI CEs, implying the most excellent electrocatalytic activity for the NiS/PANI CE in S^{2-}/S_n^{2-} redox couple, which can be logically expected considerably improved the photovoltaic performance for QDSSC.

3.3 Photovoltaic performance of QDSSCs

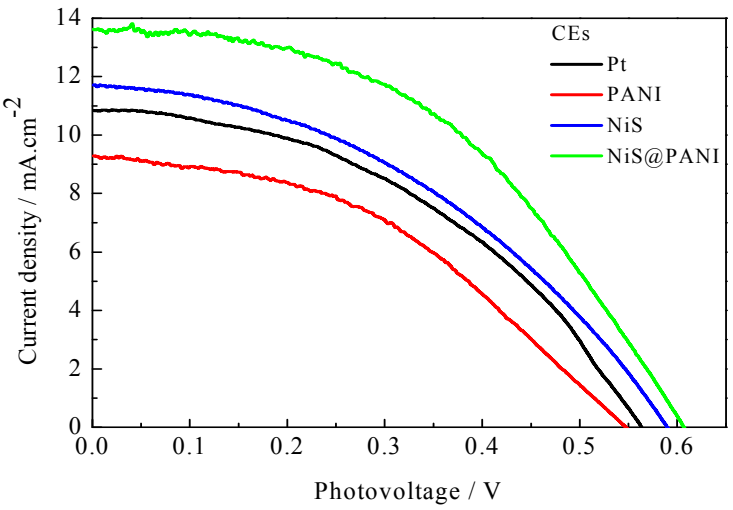

Fig. 7 *J-V* characteristics of the QDSSCs fabricated with different CEs under the standard illumination.

Fig. 7 shows the *J–V* curves of the CdSe-sensitized QDSSCs with various CEs for S^{2-}/S_n^{2-} electrolyte under the irradiation of 100 mW·cm^{-2}. The *PCEs* of the QDSSCs with the Pt, NiS, PANI and NiS/PANI CEs are 2.85%, 3.11%, 2.35% and 4.15%, respectively, and their related photoelectric performance parameters are listed in Table 2. The QDSSCs display good photovoltaic performance for the introduction of TiO_2 dense

layer and TGA modification of TiO_2, which lead to the charge recombination and fill factor improved. The QDSSCs based on the Pt and PANI CEs exhibit poor J_{sc} of 10.84 and 9.30 $mA \cdot cm^{-2}$ due to the strong absorption of S^{2-} on their surface, which reduces the surface activity of Pt and PANI. [40] The QDSSCs assembled with the NiS and NiS/PANI CEs exhibit the *PCEs* of 4.15% and 3.11%, which are higher than that of QDSSCs based on the Pt and PANI CEs. The reason for the improvement in performance for the QDSSCs possibly results from the sulfide counter electrode well matched with QDs in polysulfide electrolyte. Simultaneously, the polysulfide, adsorption on a CdSe surface, also plays as an electron acceptor to receive electron from counter electrode. Both effects are anticipated to give a better hole-recovery rate and, therefore, a higher efficiency of the device. Moreover, highly electrocatalytic activity and superior conductivity provided by the synergistic catalytic effect of the PANI and NiS, also enhance diffusion velocity for S^{2-}/S_n^{2-} redox couple as indicated in the aforementioned CV, EIS and Tafel measurements.

Table 2 The photovoltaic performance and EIS parameters of QDSSCs with various counter electrodes.

CEs	V_{oc} (V)	J_{sc} ($mA \cdot cm^{-2}$)	*FF*	*PCEs* (%)	R_s ($\Omega \cdot cm^2$)	R_{ct1} ($\Omega \cdot cm^2$)	R_{ct2} ($\Omega \cdot cm^2$)
Pt	0.56	10.84	0.47	2.85	26.35±0.01	7.61±0.01	24.61±0.01
PANI	0.55	9.30	0.46	2.35	26.10±0.01	18.44±0.01	28.72±0.01
NiS	0.59	11.71	0.45	3.11	26.54±0.01	7.28±0.01	24.75±0.01
NiS/PANI	0.61	13.62	0.50	4.15	26.70±0.01	5.39±0.01	14.76±0.01

3.4 EIS analysis of QDSSCs

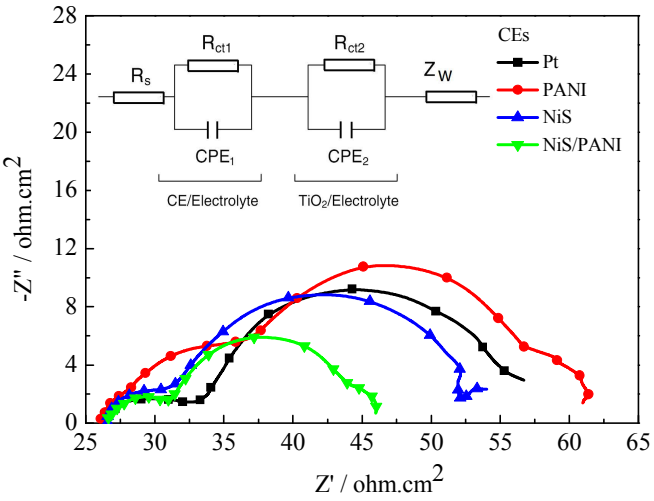

Fig. 8 EIS spectra of QDSSCs with the Pt, NiS, PANI, and NiS/PANI CEs.

The EIS of the QDSSCs based on the Pt, PANI, NiS, and NiS/PANI CEs measured under the irradiation of 100 mW·cm^{-2} and the equivalent circuit consisting of two parallel RC circuits are both showed in Fig. 8. Their corresponding values are given in Table 2, in which the R_s, the series resistance in the QDSSCs, is the nonzero intercept on the real axis of the impedance plot, which denotes the sheet resistance of transparent conductive oxide (TCO) and the contact resistance of FTO/TiO_2; R_{ct1} and R_{ct2} are the electron transfer resistances at the CE|electrolyte interface and the working electrode (WE)|electrolyte interface, respectively; Z_w in the low frequency region is attributed to the Warburg impedance of the redox couple in the electrolyte. [41] Fig. 8 and Table 2 indicate the similar R_s value of about 26.0 Ω·cm^2 for the QDSSCs with the Pt, PANI, NiS, and NiS/PANI CEs. The QDSSCs based on the Pt, PANI, NiS, and NiS/PANI CEs display the R_{ct1} of 7.61±0.01, 18.44±0.01, 7.28±0.01, and 5.39±0.01 Ω·cm^2, and corresponding to the R_{ct2} of 24.61±0.01, 28.72±0.01, 24.75±0.01, and 14.76±0.01 Ω·cm^2, respectively. The R_{ct1} and R_{ct2} for the device assembled with NiS/PANI CE exhibits the smallest value among above mention QDSSCs due to its best electrocatalytic ability in S^{2-}/S_n^{2-} electrolyte. This implies that the electrocatalytic ability of NiS/PANI CE in S^{2-}/S_n^{2-} electrolyte is much better than the others. Moreover, the smallest R_{ct2} (14.76±0.01 Ω·cm^2) value of the cell with NiS/PANI CE also obtained from Table 2, which proves the best photovoltaic performance of the device with NiS/PANI-CE once again, particularly in its *FF* (0.50) and J_{sc}. This is in consistent with the results of CV, EIS, Tafel and photoelectricity performance. These results reveal the minimum loss of internal

energy at the interface of the NiS/PANI CE and S^{2-}/S_n^{2-} electrolyte for the QDSSCs.

4. Conclusions

A QDSSC based on the NiS/PANI CE achieves a much higher power conversion efficiency of 4.15% as comparing to that of the QDSSC with Pt electrode (2.85%). The enhanced performance of the QDSSC is responsible for the excellent electrocatalytic ability and the reduced charge-transfer resistance (5.13±0.01 $\Omega \cdot cm^2$) at the CE/electrolyte interface of the cell. The electrochemical behavior to polysulfide electrolyte for the Pt, PANI, NiS, and NiS/PANI CEs are also measured made from CV, EIS and Tafel, which all show that the NiS/PANI CE possesses good catalytic behaviors and charge transport ability, and thus results in its better photovoltaic performance for the QDSSC. Furthermore, the introduction of TiO_2 dense layer and TGA modification of TiO_2 are advantageous to reduce the charge recombination and improve fill factor. Consequently, with its low cost and simplicity, we believe that the sulfide hybrid CEs have great potential for using in QDSSCs.

Authors' contributions

Gentian Yue and Furui Tan carried out the experiments, participated in the sequence alignment, and drafted the manuscript. Fumin Li, Jianming Lin and Miaoliang Huang participated in the device preparation. Weifeng Zhang and Jihuai Wu helped to draft the manuscript. All authors read and approved the final manuscript.

Acknowledgements

The authors are very grateful to the joint support by the National Natural Science Foundation of China (No.61306019) and the National Natural Science Foundation of China (No. 21103041). This work is also supported by the Natural Science Foundation of Henan Educational Committee (No. 14A430023), the Scientific Research Found of Henan Provincial Department of Science and Technology (No. 132300413210) and the Natural Science Foundation of Henan University (No. 2013YBZRO47).

References

1. A. P. Alivisatos, *Science*, 1996, **271**, 933−937.
2. J. B. Sambur, T. Novet, B. A. Parkinson, Science, 2010, **330**, 63−66.
3. M. Grätzel, *Nature*, 2001, **414**, 338−344.
4. H. Wang, Y. S. Bai, H. Zhang, Z. H. Zhang, J. H. Li, L. Guo, *J. Phys. Chem. C*, 2010, **114**, 16451−16455.
5. L. Li, X. Yang, J. Gao, H. Tian, J. Zhao, A. Hagfeldt, L. Sun, *J. Am. Chem. Soc.*, 2011, **133**, 8458–8460.
6. I. Robel, M. Kuno, P. V. Kamat, *J. Am. Chem. Soc*., 2007, **129**, 4136−4137.
7. F. R. Tan, S. C. Qu, Q. W. Jiang, J. P. Liu, Z. J. Wang, F. M. Li, G. T. Yue, S. J. Li, C. Chen, W. F. Zhang, Z. G. Wang, *Adv. Energy Mater*., 2014, **4**, 1400512.
8. J. J. Choi, Y. F. Lim, M. E. B. Santiago-Berrios, M. Oh, B. R. Hyun, L. F. Sun, A. C. Bartnik, A. Goedhart, G. G. Malliaras, H. D. Abruna, F. W. Wise, T. Hanrath, *Nano Lett*., 2009, **11**, 3749−3755.
9. S. A. Sapp, C. M. Elliott, C. Contado, S. Caramori, C. A. Bignozzi, *J. Am. Chem. Soc*., 2002, **124**, 11215−11222.
10. S. Cazzanti, S. Caramori, R. Argazzi, C. M. Elliott, C. A. Bignozzi, *J. Am. Chem. Soc*., 2006, **128**, 9996−9997.
11. P. Yu, K. Zhu, A. G. Norman, S. Ferrere, A. J. Frank, A. J. Nozik, *J. Phys. Chem. B*, 2006, **110**, 25451−25454.
12. Y. Tian, T. Tatsuma, *J. Am. Chem. Soc*., 2005, **127**, 7632−7637.
13. Y.-J. Shen, Y.-L. Lee, *Nanotechnology*, 2008, **19**, 045602.

14. R. Plass, S. Pelet, J. Krueger, M. Grätzel, U. Bach, *J. Phys. Chem. B*, 2002, **106**, 7578−7580.

15. M. K. Nazeeruddin, A. Kay, I. Rodicio, R. H. Baker, E. Muller, P. Liska, N. Vlachopoulos, M. Grätzel, *J. Am. Chem. Soc*., 1993, **115,** 6382−6390.

16. Z. Yang, C. Y. Chen, C. W. Liu, H. T. Chang, *Adv. Energy Mater*., 2011, **1**, 259−264.

17. Z. Yang, C. Y. Chen, C. W. Liu, H. T. Chang, *Chem. Commun*., 2010, **46**, 5485−5487.

18. G. Hodes, J. Manassen, D. Cahen, *J. Appl. Electrochem*., 1977, **7**, 181−182.

19. G. Hodes, J. Manassen, D. Cahen, *J. Electrochem. Soc*., 1980, **127**, 544−549.

20. S. Gime′nez, I. Mora-Sero′, L. Macor, N. Guijarro, T. Lana-Villarreal, R. Go′mez, L. J. Diguna, Q. Shen, T. Toyoda, J. Bisquert, *Nanotechnology*, 2009, **20**, 295204.

21. S.-Q. Fan, B. Fang, J. H. Kim, J.-J. Kim, J.-S. Yu, J. Ko, *Appl. Phys. Lett*., 2010, **96**, 063501.

22. G. Zhu, L. Pan, T. Xu, Z. Sun, *ACS Appl. Mater. Interfaces*, 2011, **3**, 3146–3151.

23. L. J. Sun, Y. Bai, K. N. Sun, *RSC Adv.*, 2014, **4**, 42087–42091.

24. G. T. Yue, J.H. Wu, Y.M. Xiao, M.L. Huang, J.M. Lin, J.Y. Lin, *J. Mater. Chem. A*, 2013, **1**, 1495–1501.

25. Z. L. Hu, K. Xia, J. Zhang, Z.Y. Hu, Y.J. Zhu, *RSC Adv.*, 2014, **4**, 42917–42923.

26. G. T. Yue, X. P. Ma, Q. W. Jiang, F. R. Tan, J. H. Wu, C. Chen, F. M. Li, Q. H. Li, *Electrochim. Acta*, 2014, **142**, 68–75.

27. J. H. Wu, Y. M. Xiao, G. T. Yue, Q. W. Tang, J. M. Lin, M. L. Huang, Y. F. Huang, L. Q. Fan, Z. Lan, S. Yin, T. Sato, *Adv. Mater*., 2012, **24**, 1884–1888.

28. G. T. Yue, X. A. Zhang, L. Wang, F. R. Tan, J. H. Wu, Q. W. Jiang, J. M. Lin, M. L. Huang, Z. Lan, *Electrochim. Acta*, 2014, **129**, 229–236.

29. T. Nakanishi, B. Ohtani, K. Uosakin, *J. Phys. Chem. B*, 1998, **102**, 1571–1577.

30. A. Salant, M. Shalom, Z.Tachan, S. Buhbut, A. Zaban, U. Banin, Nano Lett., 2012, **12**, 2095–2100.

31. I. V. Lightcap, P. V. Kamat, *J. Am. Chem. Soc*., 2012, **134**, 7109–7116.

32. H. Yang, W. Fan, A. Vaneski, A. S. Susha, W. Y. Teoh, A. L. Rogach, *Adv. Funct. Mater*., 2012, **22**, 2821–2829.

33. S. Licht, *Nature*, 1987, **300**, 148−151.

34. H. J. Lee, P. Chen, S.-J. Moon, F. Sauvage, K. Sivula, T. Bessho, D. R. Gamelin, P. Comte, S. M. Zakeeruddin, S. I. Seok, M. Grätzel, M. K. Nazeeruddin, *Langmuir*, 2009, **25**, 7602−7608.

35. Y.-L. Lee, C.-H. Chang, *J. Power Sources*, 2008, **185**, 584−588.

36. F. Fabregat-Santiago, J. Bisquert, E. Palomares, L. Otero, D. Kuang, M. Grätzel, *J. Phys. Chem. C*, 2007, **111**, 6550–6560.

37. E. Ramasamy, W. J. Lee, D. Y. Lee, J. S. Song, *Electrochem. Commun.*, 2008, **10**, 1087–1089.

38. Q. W. Jiang, G. R. Li, X. P. Gao, *Chem. Commun*., 2009, **44**, 6720−6722.

39. M. Wang, A. M. Anghel, B. Marsan, N.-L. Cever Ha, N. Pootrakulchote, S. M. Zakeeruddin, M. Grätzel, *J. Am. Chem. Soc*., 2009, **131**, 15976−15977.

40. H. J. Kim, D. J. Kim, S. S. Rao, A. D. Savariraj, K. S. Kyoung, M. K. Son, ChV. V. M. Gopi, K. Prabakar, *Electrochim. Acta*, 2014, **127**, 427–432.

41. S. Q. Fan, B. Fang, J. H. Kim, B. Jeong, C. Kim, J. S. Yu, J. Ko, *Langmuir*, 2010, **26**, 13644–13649.

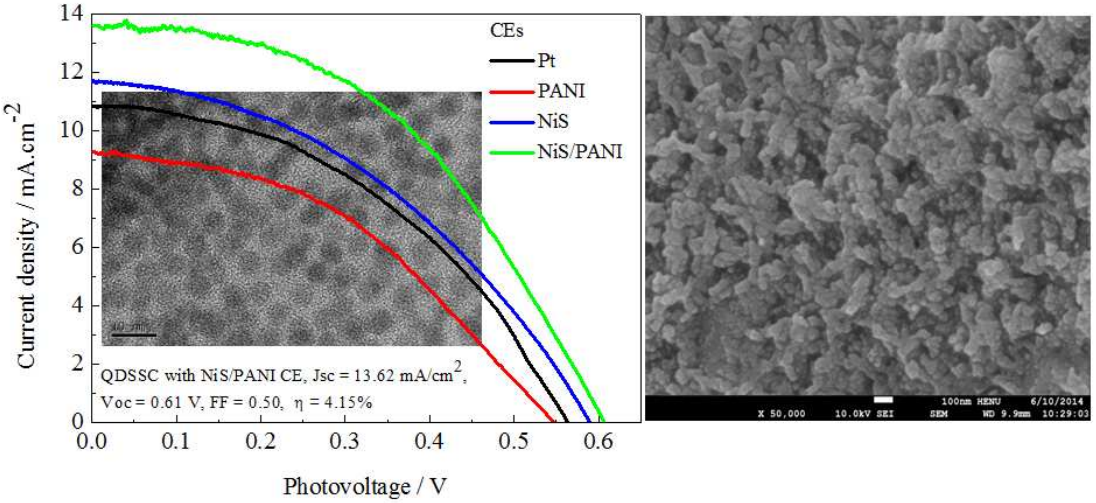

Much higher photovoltaic performance of QDSSC with CdSe QDs and NiS/PANI counter electrode.